Earthq Sci (2013) 26(3–4):223–228
DOI 10.1007/s11589-013-0034-z

The characteristics of shear wave splitting in the source region of the April 20, 2013 Lushan earthquake

Sha Liu · Jiansi Yang · Baofeng Tian · Yu Zheng · Xudong Jiang · Zhiqiang Xu

Received: 13 September 2013 / Accepted: 4 November 2013 / Published online: 5 December 2013

Abstract Using seismic data of the aftershocks sequence of the April 20, 2013 Lushan earthquake recorded by seismic temporary and permanent stations in the source region, with the visual inspection of particle motion diagrams, this paper preliminarily contains the polarization directions of fast shear wave and the time-delays of split shear waves at every station, and analyzes the crustal anisotropic characteristics in the source region. In the study area, the polarization directions at stations BAX, TQU, L132, L133, L134, and L135 are northeast, which is consistent with the strike of Dachuan–Shuangshi fault. There are two polarization directions at MDS and L131, which are northeast and southeast. The scatter of polarization directions suggests the complex stress field around these two stations where two faults intersect. For the normalized time-delays at every station, the range is 1.02–8.64 ms/km. The largest time-delay is from L134 which is closest to the mainshock, and the smallest one is from L133. The variations in time-delays show the decreasing at stations BAX, L134, and L135 because of the stress–relaxation after earthquake.

Keywords Lushan earthquake · Shear wave splitting · Polarization direction of fast shear wave · Time-delay of split shear wave

1 Introduction

The M_s7.0 Lushan earthquake on April 20, 2013 was another strong earthquake after the 2008 Wenchuan M_s8.0 earthquake on the Longmenshan faults at the eastern margin of the Tibetan Plateau, which resulted in many casualties and injuries. The epicenter of the Lushan earthquake was located at the south segment of Longmenshan fault. The depth of Lushan mainshock was 20 km, and the aftershocks occurred along the Dachuan–Shuangshi fault which was located at the southwestern end of the front range fault in the Longmenshan fault zone (Zhang et al. 2013).

Several geophysical methods have been used to monitor the seismic activity and study the geophysical background of the Lushan earthquake, which has provided a wealth of results on Lushan earthquake happening. The study on the deformation of the crust and LAB (lithosphere–asthenosphere boundary) beneath the Lushan earthquake indicates that there is strong deformation beneath the transition region from the Tibetan Plateau to Sichuan basin, which may imply the accumulation of high stresses (Shen 2013). The results of rupture process show that this earthquake is an M_w6.7 thrusting event with 159 cm largest slip. The earthquake rupture of this event occurred on the south segment of Longmenshan fault which shows increase of Coulomb stress caused by the Wenchuan earthquake (Wang et al. 2013). One view is that Lushan earthquake may be triggered by the Wenchuan earthquake, which can be considered as a delayed aftershock of Wenchuan earthquake. The rupturing process show that the rupture of the earthquake did not break through the ground surface, and the disaster is concentrated on the hanging wall of the fault (Zhang et al. 2013). The focal parameter determined by the distribution of sequences and regional stress field shows that the strike of the fault earthquake happened is 207° (Lv et al. 2013). Chi et al. (2013) argued that the strain anomalies of April 16–19 reflected the strata creeping before the rupturing of the Lushan earthquake

S. Liu (✉) · J. Yang · B. Tian · Y. Zheng · X. Jiang · Z. Xu
Institute of Geophysics, China Earthquake Administration, Beijing 100081, China
e-mail: liusha@cea-igp.ac.cn

generating fault. To get a more comprehensive and profound understanding of the anisotropic distribution in Lushan area, we use shear wave splitting to monitor seismic activity and evaluate the stress changes associated with the earthquake happening. In this paper, we show the behavior of stress field in the source region determined by the shear wave splitting.

Shear wave splitting (SWS), analogous to optical birefringence, caused by the azimuthal anisotropy of stress-aligned fluid-filled microcracks and aligned pore spaces, is observed for propagation through almost all sedimentary, igneous, and metamorphic rocks in the crust (Crampin 1994; Crampin and Peacock 2005, 2008; Crampin and Gao 2006). Changes in SWS monitor stress-induced changes to the fluid-saturated stress-aligned microcracks pervading almost all rocks in the Earth's crust (Crampin et al. 2008). The microcracks are very sensitive to changes of stress and the microcrack geometry responds to even low-level changes of tectonic stress by modifying microcrack aspect ratios. Observation of SWS at the surface indicates that the polarization direction of the fast shear wave is generally parallel to the local direction of maximum horizontal stress in the crust (Crampin 1999a). The stress changes in the crust can be monitored by measuring time-delays between split shear waves along suitable ray paths (Crampin 1999b). Using persistent swarms of small earthquakes as the source of shear waves, characteristic patterns of variations of SWS time-delays have been recognized, retrospectively, before 15 earthquakes worldwide ranging in magnitude from a M1.7 swarm event in Iceland to the 2004 M9.2 Sumatra–Andaman earthquake in Indonesia (Crampin and Gao 2012). The recent studies also suggest that there is a close relationship between the characteristics of SWS and the nature of the fault. Therefore, the SWS can be used to study the local crustal anisotropy, stress field, and the fracture properties (Peng and Ben-Zion 2004; Shi et al. 2006; Wu et al. 2007).

2 Data and method

2.1 Seismic activity

After the occurrence of the Lushan earthquake, the aftershock sequence developed, and the number of aftershock is above 5,000 until the end of April. To monitor the seismic activity, China Earthquake Administration placed 15 temporary seismic stations in the source region to record thousands of aftershocks. We use different colors to show the different earthquakes from April 20 to May 2 (Fig. 1). The most aftershocks occurred along the Dachuan–Shuangshi fault which situates at the southwestern end of the front range fault in the Longmenshan fault zone.

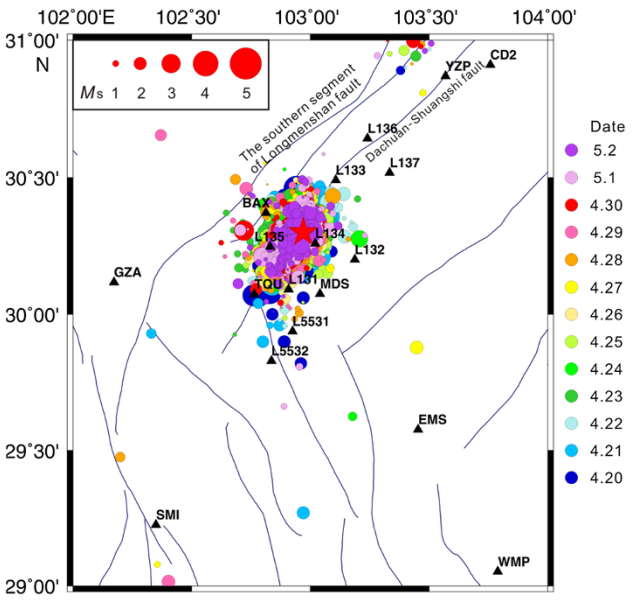

Fig. 1 Distribution of aftershocks of the Lushan earthquake and the seismic stations. *Colored circles* are the locations of the aftershocks, and *triangles* are seismic stations

The magnitudes of most aftershocks are between 1.0 and 3.0 with the largest one being M_s5.7 earthquake in April 20. In the spatial distribution of aftershocks, the aftershocks distributed widely and much more concentrated in the southwest of mainshock, which indicates that the aftershocks expanded in the southwest direction (Fig. 1). The relocation of the aftershocks suggests that the extension is predominated in southwestward direction about 23 km but is the weak in the northeastward direction around 12 km, which is not a simple unilateral rupture (Zhang et al. 2013).

2.2 Method

The purpose of SWS is to separate the fast and slow shear wave from the seismic data. There are two parameters of SWS, polarization directions and time-delays. A variety of techniques have been developed to measure the polarization directions and time-delays of seismic SWS. Visual inspection of particle motion diagrams is subjective but is probably most accurate (Crampin and Gao 2006). In this paper, we analyze the particle motion diagrams to get the parameters of SWS. All shear wave arrivals within the shear wave window show abrupt changes in direction of particle motion strongly diagnostic of some form of anisotropy-induced SWS. We cannot accurately judge the shear wave arrivals because of the complexity of the shear wave. We choose 20 sample points before and 40 sample points after possible shear wave arrivals in three 20-sample polarization diagrams (Fig. 2). The polarization directions of shear waves up to the first abrupt change of direction are

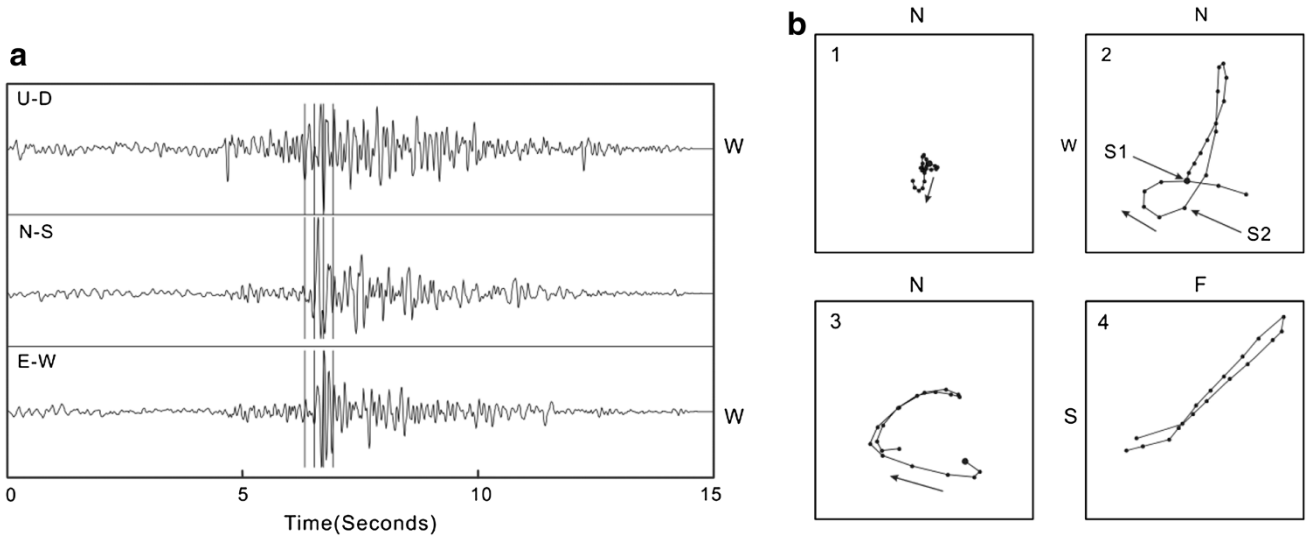

Fig. 2 Measurement of SWS time-delays on horizontal polarization diagrams at Station BAX. **a** Three-component seismograms at 100 samples-per-second of M_s 1.2 earthquake at April 22, 2013, with three 0.2 s, 20 samples, time intervals marked starting 20 samples before the shear wave arrival. **b** The four polarization diagrams of the shear wave in the same scale; (1) polarization diagram of 20 samples before shear wave arrival; (2) polarization diagram of 20 samples after shear wave arrival; (3) polarization diagram of the next 20 samples; (4) the polarization diagram of fast wave and slow wave after delay time correction

Table 1 The parameters of shear wave splitting at stations in Lushan region

Station	Lat (°)	Lon (°)	DD	*N*	φ (°)	$\Delta\varphi$ (°)	dt (ms/km)	Adt (ms/km)	Δdt (ms/km)
BAX	30.4	102.8	April 20–May 1	172	66	39.5	1.04–7.19	3.68	1.19
MDS	30.1	103.0	April 20–May 1	16	98	36.2	1.25–6.07	3.18	1.52
TQU	30.1	102.8	April 20–May 1	35	81	27.3	1.59–5.93	3.74	1.45
L131	30.1	102.9	April 22–May 1	24	72	35.4	2.09–6.28	4.58	1.64
L132	30.2	103.2	April 22–May 1	3	25	11.8	1.42–5.06	3.46	1.85
L133	30.5	103.1	April 22–May 1	2	16	7.1	1.02–3.85	2.43	2.00
L134	30.3	103.0	April 22–May 1	123	74	34.5	2.35–8.64	4.35	1.23
L135	30.2	102.8	April 22–May 1	92	57	40.2	1.61–6.79	4.31	0.98

DD is the duration of the seismic data; *N* is the number of earthquake events within SWW; φ is the mean polarization directions of the fast shear wave; $\Delta\varphi$ is the standard error of the polarization directions; dt is the range of time-delays at every station; Adt is the average value of time-delays at every station; Δdt is the standard error of time-delays at every station

assumed to be the polarization directions of the fast split shear wave. The arrivals of slow shear waves were also characterized by the abrupt changes in the direction of the polarization diagrams. In most records, however, the arrivals of shear wave could not be picked up accurately, because of the disturbance by other P generated.

In this study area, several temporary and permanent seismic stations recorded over 5,000 earthquake catalogs until the end of May 2 at a sampling rate of 100 sps (Fig. 1). Using SWS to study the crustal anisotropy, the quality of observational seismic data must be high relatively. First, we should choose the seismic data within the effective shear wave window (SWW). The three-component waveforms of shear waves recorded at a free-surface are similar to the incidence waveforms only within SWW. Then, the signal-to-noise ratio of the data should be large relatively. To eliminate the effects of severe shallow irregularities, especially surface low velocity layer, we choose the earthquakes within SWW of 45° with signal-to-noise ratios S/N >8.0. Only 3 permanent stations (BAX, MDS, and TQU) and 5 temporary stations (L131, L132, L133, L134, and L135) recorded numbers of seismic events within SWW (Table 1).

After data choosing and SWS computing, we get 467 results of SWS parameters using the data from 8 seismic stations in the source region. These parameters are different at different stations, which reveals the changes of the crack geometry and the characteristics of the stress distribution. Then, we will discuss the characteristics of the SWS parameters in the source region of Lushan earthquake.

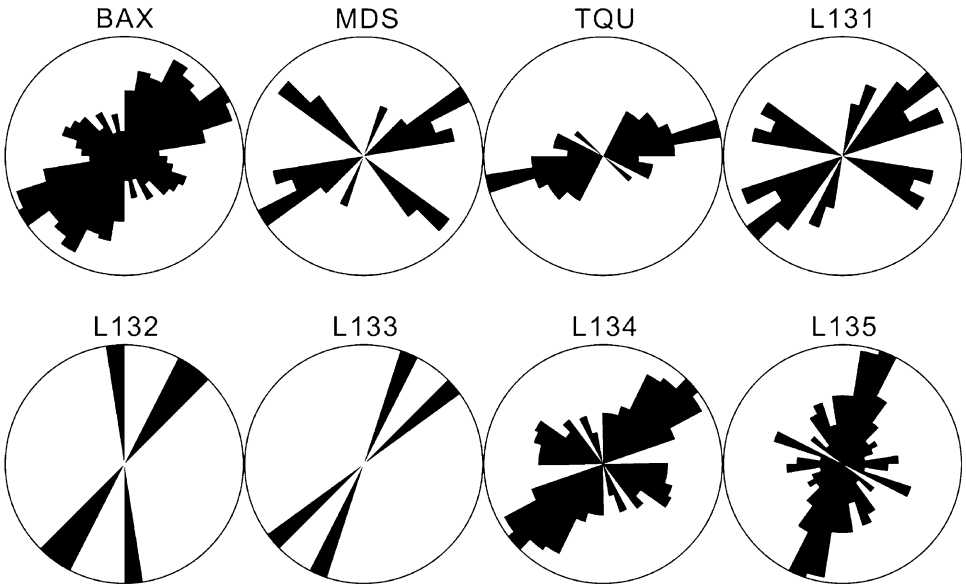

Fig. 3 The homolographic projection rose diagrams of the polarization directions of the fast shear wave splitting at 8 seismic stations

3 Results of polarization directions

By the analysis of SWS at the 8 seismic stations in the source region, we get the polarization directions at every seismic station, which is in good consistency with minimal scatter (Fig. 3). The homolographic projection rose diagrams of the polarizations suggest that the polarization directions of the fast shear wave are obvious, although several stations show complex polarization directions. For example, there are two polarization directions at station MDS. Table 1 shows the values and the errors of the SWS parameters at every station. Although at station L133 there are only two polarizations results with small error, the polarization directions are the same as that of other stations, which confirms the reliability of the results further.

From the polarization directions of the stations around the Dachuan–shuangshi fault (Fig. 4), the spatial distribution of the regional stress direction is revealed. In the northern part of the study area, station L133 shows northeast polarization direction, which is consistent with the strike of fault. Although stations BAX, L135 and stations L134, L132 are located on the both sides of the fault, the polarization directions at these four seismic stations are in northeast direction with one accord. In the southern part, the polarization directions of fast waves show some scatter at station TQU and station L131, MDS in both sides of the fault. TQU show northeast direction in polarizations. But there are two polarization directions in L131 and MDS, which are northeast and southeast.

The polarization directions of the faster split shear waves are typically parallel to the strike of microcracks and parallel to the direction of the maximum horizontal

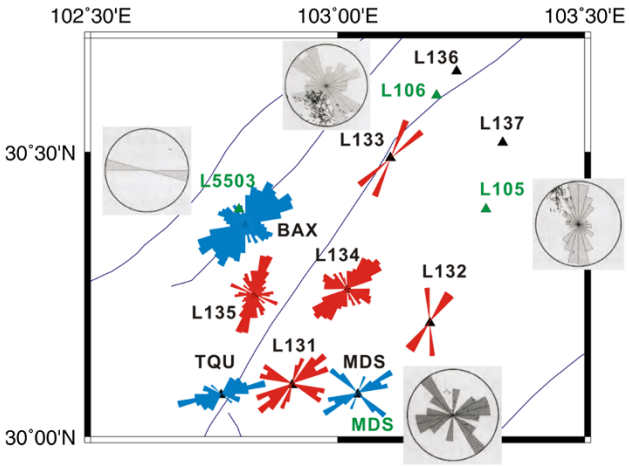

Fig. 4 The distribution of the homolographic projection rose diagrams at stations in the study area; The *blue* results are from the stations of the regional permanent seismic network; the *red* results are from the temporary seismic stations. The *green* stations and the *shadows* are from the results of Wenchuan earthquake (Shi et al. 2009)

compressional stress (Crampin 1994; Crampin and Peacock 2005, 2008; Gao et al. 2011). This is because microcracks open normal to the direction of minimum compressional stress, which is typically horizontal, so microcracks are usually aligned vertically parallel to the direction of maximum horizontal stress (Crampin 1999a). Therefore, in the study area, the maximum horizontal compressional stress is in the northeast direction. The strike of Dachuan–shuangshi fault is northeast, which is in agreement with the polarization directions of fast shear waves.

The northeast direction in the regional stress field has been retrospectively observed in the southern segment of

Longmenshan fault in other geophysical studies. The strike of the Longmenshan fault is in northeast direction, which is the same as the direction of the stress field. Comparing the results of seismic anisotropy of Wenchuan earthquake sequence, there are some differences in polarization directions between these two earthquakes (Fig. 4) (Shi et al. 2009; Gao et al. 2013). L106 shows northeast and northwest polarization directions, and L105 shows nearly north polarization direction which is the same as that at L132. There is only one result at station L5503, which is nearly E–W direction. Although L5503 is close to BAX, the polarization directions are different at those two stations. At station MDS, there are two polarization directions in our results, northeast and southeast, which is in good agreement with the results from Wenchuan earthquake (Shi et al. 2013; Gao et al. 2013). The polarization directions of fast shear wave are determined by the microcracks in the crust which are sensitive to the stress. Lushan earthquake is a thrusting event, and Wenchuan earthquake is a thrusting event with strike-slip component (Zhang et al. 2009). Furthermore, the epicenter distance of these two earthquakes is 90 km, and there is a rupture blank zone of 60 km in length between the two earthquakes (Gao et al. 2013), so the results of polarization directions in these two earthquakes are driven by the regional stress with different characteristics.

4 Variations of time-delays between split shear waves

The time-delay between split shear waves is a quantity of the anisotropic degree. To compare and analyze the variations of time-delays, we normalized the time-delays using the length of ray path between the station and the source (Liu et al. 2012). The time-delays in our study area are in the range of 1.02–8.64 ms/km (Table 1), and the average value is 3.89 ms/km with the standard error 1.23 ms/km. The largest time-delay is from L134 which is closest to the mainshock, and the smallest one is from L133. There is some scatter in the results of time-delays. However, the large scatter ("±80 %") typically also observed in SWS time-delays from other small earthquakes, is attributed to the critically high pore-fluid pressures on all seismically active fault planes (Crampin 1999a, b; Crampin et al. 2004).

To analyze the temporal variations of time-delays, we choose the results at stations BAX, L134, and L135 because of a great many earthquakes within SWW (Fig. 5). From the results of 9-point moving average, there are some variations in time-delays. The time-delays show a significant decreasing after the main shock until the end of April 23 at station BAX. From April 24 to May 1, there is a hardly noticeable decreasing in time-delay. At stations

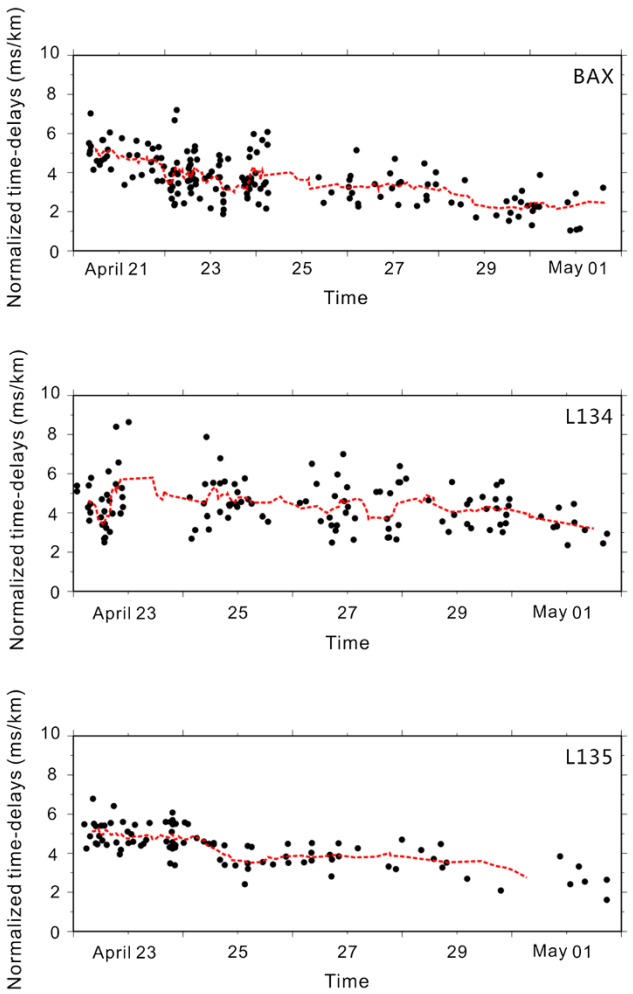

Fig. 5 Changes in time-delays at BAX, L134, and L135 stations, respectively. The *black dots* are the results of time-delays from all the earthquakes within SWW. The *red dashed line* is the result of 9-point moving average

L134 and L135, the time-delays reveal a decreasing from April 22 as a whole. Similar decreasing in time-delays has also been observed after Wenchuan earthquake (Ding et al. 2008), and other earthquakes in the world (Crampin et al. 1990; Crampin and Gao 2005, 2012; Gao et al. 1998; Gao and Crampin 2004), showing that the behavior of stress is very similar after earthquakes. Time-delays are sensitive to crack aspect rations and hence stress change. Here, the characteristic decreasing in time-delays is interpreted as stress–relaxation decreases as microcracks coalesce onto the eventual fault plane for earthquakes.

5 Conclusions

We got the results of SWS from the seismic data recorded by the seismic permanent and temporary stations in the source region of Lushan earthquake. The SWS parameters are

obtained by the method of visual inspection of particle motion diagrams. The polarization directions at stations BAX, TQU, L132, L133, L134, and L135 are northeast, which are consistent with the strike of Dachuan–Shuangshi fault. There are two polarization directions at stations MDS and L131, which are northeast and southeast. The scatter of polarization directions suggests the complex stress field around these two stations where two faults intersect. The polarization directions in our results are slightly different from that in Wenchuan earthquake, which reveals different characteristics of the regional stress field between these two earthquakes.

We also obtain the normalized time-delays at every station. The range of time-delays is 1.02–8.64 ms/km. The largest time-delay is from L134 which is closest to the mainshock, and the smallest one is from L133. We observed the decreasing in time-delays at stations BAX, L134, and L135 after the main shock because of the stress–relaxation after earthquake. By analyzing SWS around the source region of Lushan earthquake, we conclude that the observed distribution of polarization directions and the variations of time-delays reflect a fundamental anisotropic characteristic in the crust.

Acknowledgments The authors thank Earthquake Administration of Sichuan Province, China for providing data used in our study. This work was supported by Research Project in Earthquake Science (Nos. 201308018 and No. 201108002) and National Natural Science Foundation of China (No. 40904012).

References

Chi SL, Liu Q, Chi Y, Deng T, Liao CW, Yang G, Zhang GP, Chen J (2013) Borehole strain anomalies before the 20 April 2013 Lushan Ms 7.0 earthquake. Acta Seismol Sin 35(3):296–303

Crampin S (1994) The fracture criticality of crustal rocks. Geophys J Int 118:428–438

Crampin S (1999a) Calculable fluid-rock interactions. J Geol Soc 156:501–514

Crampin S (1999b) Stress-forecasting earthquakes. Seismol Res Lett 70:291–293

Crampin S, Gao Y (2005) Comment of on 'systematic analysis of shear-wave splitting in the aftershock zone of the 1999 Chi–chi earthquake: shallow crustal anisotropy and lack of precursory variations', by Liu, Y, Teng, T.-L., & Ben Zion, Y. Bull Seismol Soc Am 95:354–360. doi:10.1785/0120040092

Crampin S, Gao Y (2006) A review of techniques for measuring shear-wave splitting above small earthquakes. Phys Earth Planet Inter 159:1–14

Crampin S, Gao Y (2012) Plate-wide deformation before the Sumatra–Andaman earthquake. J Asian Earth Sci 46:61–69

Crampin S, Peacock S (2005) A review of shear-wave splitting in the compliant crack-critical anisotropic earth. Wave Motion 41:59–77

Crampin S, Peacock S (2008) A review of the current understanding of seismic shear-wave splitting in the earth's crust and common fallacies in interpretation. Wave Motion 45:675–722

Crampin S, Booth DC, Evans R, Peacock S, Fletcher JB (1990) Changes in shear wave splitting at Anza near the time of the North Palm Springs earthquakes. J Geophys Res 95:11197–11212

Crampin S, Peacock S, Gao Y, Chastin S (2004) The scatter of time-delays in shear-wave splitting above small earthquakes. Geophys J Int 156:39–44

Crampin S, Gao Y, Peacock S (2008) Stress-forecasting not predicting earthquakes: a paradigm shift? Geology 36:427–430

Ding ZF, Wu Y, Wang H, Zhou XF, Li GY (2008) Variations of shear wave splitting in source region of 2008 Wenchuan earthquake. Sci China 38(12):1600–1604 (in Chinese with English abstract)

Gao Y, Crampin S (2004) Observations of stress relaxation before earthquakes. Geophys J Int 157:578–582

Gao Y, Wang P, Zheng S, Wang M, Chen YT, Zhou H (1998) Temporal changes in shear-wave splitting at an isolated swarm of small earthquakes in 1992 near Dongfang, Hainan Island, southern China. Geophys J Int 135:102–112

Gao Y, Wu J, Fukao Y, Shi YT, Zhu AL (2011) Shear-wave splitting in the crust in North China: stress, faults and tectonic implications. Geophys J Int 187(2):642–654

Gao Y, Wang Q, Zhao B, Shi YT (2013) A rupture blank zone in middle south part of Longmenshan Faults: effect after Lushan Ms 7.0 earthquake of 20 April 2013 in Sichuan, China. Sci China Earth Sci 43(6):1038–1046

Liu S, Yang JS, Tian BF, Zheng Y, Jiang XD, Xu ZQ (2012) Characteristics of crustal anisotropy beneath the Yushu region. Chin J Geophys 55(10):3327–3337 (in Chinese with English abstract)

Lv J, Wang XS, Su JR, Pan LS, Li Z, Yin LW, Zeng XF, Deng H (2013) Hypocentral location and source mechanism of the Ms 7.0 Lushan earthquake sequence. Chin J Geophys 56(5):1753–1763. doi:10.6038/cjg20130533 (in Chinese with English abstract)

Peng Z, Ben-Zion Y (2004) Systematic analysis of crustal anisotropy along the Karadere–Duzce branch of the North Anatolian fault. Geophys J Int 159:253–274

Shen XZ (2013) An analysis of the deformation of the crust and LAB beneath the Lushan and Wenchuan earthquakes in Sichuan province. Chin J Geophys 56(6):1895–1903. doi:10.6038/cjg20130612 (in Chinese with English abstract)

Shi YT, Gao Y, Wu J, Luo Y, Su YJ (2006) Seismic anisotropy in crust in Yunnan-preliminary study on polarization of fast shear wave. Acta Seismol Sin 28(6):574–585 (in Chinese with English abstract)

Shi YT, Gao Y, Zhao CP, Yao ZX, Tai LX, Zhang YJ (2009) A study of seismic anisotropy of Wenchuan earthquake sequence. Chin J Geophys 52(2):398–407 (in Chinese with English abstract)

Shi YT, Gao Y, Zhang YJ, Wang H, Yao ZX (2013) Shear-wave splitting in the crust in Eastern Songpan–Garze block, Sichuan–Yunnan block and Western Sichuan Basin. Chin J Geophys 56(2):481–494 (in Chinese with English abstract)

Wang WM, Hao JL, Yao ZX (2013) Preliminary result for rupture process of Apr. 20, 2013, Lushan earthquake, Sichuan, China. Chin J Geophys 56(4):1412–1417. doi:10.6038/cjg20130436 (in Chinese with English abstract)

Wu J, Gao Y, Chen YT, Huang JL (2007) Seismic anisotropy in the crust in northwestern capital area of China. Chin J Geophys 50(1):209–220 (in Chinese with English abstract)

Zhang Y, Xu LS, Chen YT (2009) Spatio-temporal variation of the source mechanism of the 2008 great Wenchuan earthquake. Chin J Geophys 52(2):379–389 (in Chinese with English abstract)

Zhang Y, Xu LS, Chen YT (2013) Rupture process of the Lushan 4.20 earthquake and preliminary analysis on the disaster-causing mechanism. Chin J Geophys 56(4):1408–1411. doi:10.6038/cjg20130435 (in Chinese with English abstract)